Fusion Engineering and Design 194 (2023) 113729

Contents lists available at ScienceDirect

Fusion Engineering and Design

journal homepage: www.elsevier.com/locate/fusengdes

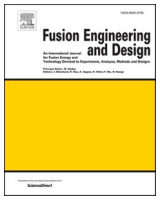

Thermal-hydraulic optimization of a proposed EU-DEMO hydrogen passive removal system

T. Glingler, G. Caruso, M. D'Onorio *

Sapienza University of Rome, Department of Astronautical, Electrical and Energy Engineering (DIAEE)– Nuclear Section Corso Vittorio Emanuele II 244, 00186 Roma, Italy

A B S T R A C T

As the R&D of magnetic fusion power demonstrating plants are approaching important steps toward concept designs, analysts are working parallelly on the safety assessment of such concepts to identify any potential risk. One of the safety concerns involves the confinement of radioactive substances during normal operation and accidental conditions. Several accident sequences inside the tokamak vacuum vessel or pressure suppression systems are characterized by the risk of hydrogen buildup and subsequent ignition that could threaten the structural confinement integrity. In the Safety and Environment work package of the EUROfusion consortium, possible approaches to mitigate the hydrogen explosion risk are under investigation. One of the exploratory solutions is based on limiting the hydrogen concentration that could reach flammable gas mixture conditions and using Passive Autocatalytic Recombiners (PARs) installed into the atmosphere of the pressure suppression systems tanks to recombine hydrogen.

This paper examines the theoretical effectiveness of the PARs intervention during an in-vessel loss of coolant accident without the intervention of the decay heat removal system for the Water-Cooled Lithium Lead (WCLL) concept of EU-DEMO, using an optimization methodology. The involved systems have been modelled in MELCOR to estimate the PARs recombination capability as a function of the thermal-hydraulic parameters of the suppression tanks. Furthermore, the optimizer entity of the RAVEN tool is applied to perform optimization studies on the hydrogen recombination system design parameters. The goal is to explore the geometrical and thermal-hydraulic parameters that maximize the capability of the hydrogen removal system for the WCLL concept.

1. Introduction

In the framework of the EUROfusion Work Package Safety And Environement (WPSAE), analysts are supporting the design activities to ensure that those conceptual designs satisfy the safety requirements regarding the personnel, public and environment [1,2]. An extended number of initiating events have been selected to demonstrate the plant response to a set of reference accident sequences [3]. One of the main Design Basis Accident (DBA) analyzed for DEMO is the in-vessel Loss of Coolant Accident (LOCA) for the WCLL blanket concept [4,5].

The current design data adopted are referred to the WCLL 2018 design, shown in detail in Table 1. Power parameters have been used for the modeling activities associated to the PHTS.

A high energy content characterizes the primary cooling system, whose main data is provided in Table 2, due to the pressurized water coolant (15.5 MPa), and when it is released into the Vacuum Vessel (VV), it causes an over-pressurization that may damage the VV internals. Since the VV has a confinement function for radioactive releases during normal and accidental conditions, its integrity must be guaranteed by maintaining pressure below 0.2 MPa as a safety standard [8]. A prominent solution to safely mitigate the VV overpressure due to in-vessel LOCA events is based on the Vacuum Vessel Pressure Suppression System (VVPSS). The VVPSS is a passive safety system that relies on the suppression of steam released in the VV during LOCAs, and due to its importance, it has been temporarily classified as a SIC-1 system [9].

This work is based on the preliminary sizing of the main thermo-hydraulic and geometrical parameters of the VVPSS described in [10, 11]. The cited analyses successfully demonstrate the VVPSS capability to protect the VV from overpressure, keeping the maximum value under the design limit equal to 0.2 MPa. Another primary function of the VVPSS is to demonstrate its effectiveness in mitigating hydrogen explosion risk [12]. The hydrogen explosion could represent a risk since it can cause a direct over-pressurization of the VV and source term mobilization [13].

The solutions adopted for hydrogen mitigation in fission technologies could not be applicable in fusion reactors since the VV and VVPSS operational pressure are significantly different. The present work aims to demonstrate the capabilities of the PARs as a hydrogen mitigation system in the fusion devices and to optimize some specific parameters of

* Corresponding author.
E-mail address: matteo.donorio@uniroma1.it (M. D'Onorio).

https://doi.org/10.1016/j.fusengdes.2023.113729
Received 3 October 2022; Received in revised form 3 April 2023; Accepted 4 April 2023
Available online 7 April 2023

Table 1
DEMO WCLL BB power balance [6,7].

Parameter	Units	Value
Total Nuclear Heating	MW	1650.3
Total FW Heat Flux (HF)	MW	272.7
Av. FW Heat Flux	MW/m^2	0.22
Total FW Power	MW	439.8
Total BZ Power	MW	1483.2
Total Reactor Power	MW	1923.2

Table 2
WCLL BB cooling system parameters [6,7].

Parameter	Units	Value
Typology of coolant	–	Water
Pressure	MPa	15.5
Temperature Range	°C	295–328
Av. Coolant Density	kg/m^3	701.3
FW PHTS flow rate	kg/s	2271.6
BZ PHTS flow rate	kg/s	7661.2
Total flow rate	kg/s	9936.0

the VVPSS to increase the hydrogen mass recombined within the design specification already assessed.

The optimization methodology needs the integration between a system code capable of replicating the accident scenario and a front-end code that executes the optimization algorithm. MELCOR and RAVEN have been coupled through a Python script to perform the optimization methodology, studying the final amount of H_2 recombined in each run and searching for the optimal design and thermal-hydraulic parameters that increase the mass recombined. RAVEN is a software tool developed at the Idaho National Laboratory (INL) to act as a control logic driver and post-processing tool for different applications [14–18]. MELCOR for fusion is a fully integrated design basis and severe accident code that simulates thermal-hydraulic behavior and self-consistently accounting for aerosol transport in nuclear facilities and reactor cooling systems to evaluate the source term in fusion reactors [19,20]. The optimization algorithm adopted is based on the gradient descent methodology, computing the local gradient with the central difference approach.

The accident selected to perform this study is a Double Ended Guillotine Break (DEGB) of 10 Outboard First Wall (OB-FW) cooling channels, for a total break area of 0.00098 m^2, during a plasma burn phase with resulting in-vessel LOCA. The unmitigated disruption is assumed to affect 2 different outboard segments causing the additional break of 262 First Wall (FW) channels, for a total break area of 0.02568 m^2.

2. Optimization methodologies

Optimization methodologies are used to find the optimal value of a goal function. The process consists of searching for the best-fitted combination of the variables that affect the goal function within a specified set of boundary conditions. The mathematical approach of optimization techniques could be based on both deterministic and stochastic approaches [21].

The most common deterministic methods rely on local gradient calculations. The objective function domain is explored, verging on reducing the local gradient. For linear spaces, deterministic approaches are efficient and effective [22,23]; while when applied to problems with non-linear search spaces, these methods could be trapped around local optima without searching the global domain entirely [24,25].

Stochastic approaches explore the domain globally, generating random dependencies for the objective function. The stochastic nature outlines the independency of the derivative information of the problem [26]. This characteristic gives a significant advantage when searching non-linear problems without being concerned with local optima entrapment. Another advantage is the adaptability of the algorithm to a wide range of problems. Stochastic algorithms treat the optimization problem from outside of the mathematical dependencies that characterize the objective function. This permits the stochastic algorithm to be independent from the problem and be easily adaptable to diverse optimal searches. The counterpart of the stochastic algorithm relies on an approximate evaluation of local maximum and minimum. The global search of the domain helps to find all those regions where the highest or lowest value of the objective function is located. However, it does not directly search the local maximum or minimum in those regions.

The hybrid algorithms, which incorporate both deterministic and stochastic methods, benefit from both procedures and advantages [25]. Exploration and exploitation are two consecutive features of hybrid algorithms [21]. Exploration of the global domain through stochastic approaches allows to escape from local optima entrapment. The result of the exploration is to find optimal candidates to be analyzed in the global domain in a consequent step: the information gained in the first step of the algorithm are adopted to initialize the exploitation feature. Using a deterministic approach, the exploitation operates a precise search in the microdomain of the optimal candidates found in the previous step. The efficient and precise characteristics of deterministic approaches increase the accuracy of the optimal candidates found through stochastic analysis. Hybrid algorithms overcome the limits of deterministic and stochastic approaches reaching complete and detailed research of the goal function optima.

2.1. RAVEN gradient descent optimizer

One of the optimization algorithms embedded in the RAVEN tool is based on the Gradient Descent method. It is a deterministic approach based on various gradient estimation techniques, stepping strategies, and acceptance criteria. The algorithm works by estimating locally the gradient of the objective function. Each new consequent search tends to decrease the gradient value, changing a set of predefined parameters of the objective function. Once all the acceptance criteria are reached, then the algorithm is considered converged. Multiple initial parallel trajectories are needed to obtain a global solution that overcomes entrapment in local minima.

Several gradient estimation techniques could be applied to the optimizer algorithm (e.g., Finite Difference, Central Difference, Simultaneous Perturbation Stochastic Approximation (SPSA)). The Finite Difference uses orthogonal perturbations in each input space dimension to estimate the local gradient. It requires a total of N perturbations, where N is the dimensionality of the input space. Given the input space $\boldsymbol{i} = (x, y, z)$ that defines the objective function $f(i)$, then the algorithm chooses three perturbations (α, β, γ). Consequently, it evaluates the following perturbation points:

- $f(x + \alpha, y, z)$;
- $f(x, y + \beta, z)$;
- $f(x, y, z + \gamma)$.

The next step evaluates the gradient $\nabla f = (\nabla^{(x)}f, \nabla^{(y)}f, \nabla^{(z)}f)$ as:

$$\nabla^{(x)}f \approx \frac{f(x+\alpha, y, z) - f(x, y, z)}{\alpha}$$

and also, for $\nabla^{(y)}f$ and $\nabla^{(z)}f$.

The Central Difference is similar to the Finite Difference approximation; it differs by using a pair of orthogonal perturbations in each dimension of the input space instead of only one. Using the same input space example as before, $\boldsymbol{i} = (x, y, z)$ and $f(i)$ as the objective function, RAVEN evaluates the following perturbation points:

- $f(x \pm \alpha, y, z)$;
- $f(x, y \pm \beta, z)$;
- $f(x, y, z \pm \gamma)$.

The next step evaluates the gradient $\nabla f = (\nabla^{(x)}f, \nabla^{(y)}f, \nabla^{(z)}f)$ as:

$$\nabla^{(x)}f \approx \frac{f(x+\alpha,\ y,\ z) - f(x,\ y,\ z)}{2\alpha}$$

and also, for $\nabla^{(y)}f$ and $\nabla^{(z)}f$.

The SPSA approximation differs from the previous methods. It adopts a single perturbation as a zeroth-order gradient approximation, regardless of the dimensionality of the input space. Given the input space $\boldsymbol{i} = (x, y, z)$ that defines the objective function $f(\boldsymbol{i})$, then the SPSA chooses one perturbation point $(\epsilon^{(x)}, \epsilon^{(y)}, \epsilon^{(z)})$. Consequently, it evaluates the following perturbation point:

$$f\left(x+\epsilon^{(x)},\ y+\epsilon^{(y)},\ z+\epsilon^{(z)}\right);$$

The next step evaluates the gradient $\nabla f = (\nabla^{(x)}f, \nabla^{(y)}f, \nabla^{(z)}f)$ as:

$$\nabla^{(x)}f \approx \frac{f\left(x+\epsilon^{(x)},\ y+\epsilon^{(y)},\ z+\epsilon^{(z)}\right) - f(x,\ y,\ z)}{\epsilon^{(x)}}$$

and also, for $\nabla^{(y)}f$ and $\nabla^{(z)}f$. It has the benefit of being independent from the dimensionality of the input space, although is less robust than the previous methods.

Until the acceptance criteria have not been met, the optimization process needs to search the input space for new optimal candidates. All three approximations utilize a user-defined scalar to define at which distance from the optimal point the perturbation should evaluate the gradient. This scalar is also a multiplier for the step size used to reach the new optimal candidate from the previously calculated optimal point. To improve the search for new optimal points, RAVEN adopts different iterative stepping algorithms: the Gradient History and the Conjugate Gradient. These algorithms adaptively choose how long the step size has to be along a search path.

The Gradient History algorithm evaluates the step size using the sequential change of the gradient during the optimization process. It considers the directional change of the gradient versor and adaptively chooses a larger or smaller step size. Based on the gradient value between two consecutive steps and on the previous search history, the step size grows if the direction taken decreases the gradient value. While if the gradient between two consecutive steps changes direction, the step size shrinks. The algorithm uses two variables, the shrink and growth factor. These values manage the rate of growth and shrink of the step size.

3. DEMO modeling description

DEMO Primary Heat Transfer System (PHTS) and VVPSS have been modeled in MELCOR to simulate the thermal-hydraulic phenomena during steady and transient conditions. The MELCOR model developed has been performed using a modified version of the MELCOR 1.86 code [19,20]. INL developed this fusion-adapted version to improve the code modeling capability of fusion reactors.

3.1. PHTS

The model has been developed following the data provided in [27]. The PHTS is divided between two loops, one concerning the Breeding Zone (BZ) and the second concerning the FW; each is then divided between the in-vessel and the ex-vessel section. The BZ loop is connected to a pressurizer, operating at a nominal pressure of 15.5 MPa, with a total volume of 101.26 m^3 filled with 44.8 m^3 of water. At the same time, the FW-PHTS pressurizer has a total volume of 39.29 m^3 and contains 18.2 m^3 of liquid water. The total inventory of water considering both in-vessel and ex-vessel components is 200.8 m^3 and 545.5 m^3 for the FW-PHTS and BZ-PHTS, respectively.

The ex-vessel section of both loops includes: steam generators, pump systems, and the hot and cold distributor ring. Both the hot and cold distributors have been modeled in 4 control volumes; each one of those is connected to three in-vessel regions described in the following paragraph.

The in-vessel region of the DEMO reactor has been modeled in three different regions simulating: 1 sector (which modules trigger the accident sequence), a group of 7 sectors, and a group of 8 sectors. Each sector has been divided into an inboard and outboard segment. Water enters and exits each sector through the inlet and outlet feeding pipes, connecting the BM manifold with ring distributors connected to the steam generators through hot and cold legs. The inlet and outlet pipes are placed at the center of the manifolds and at the top of the manifolds for the outboard segment and inboard segments, respectively. Fig. 1 shows the MELCOR nodalization scheme of the PHTS.

3.2. DEMO vacuum vessel

The EU-Demo Vacuum Vessel has been modeled with control volumes connected by open flow paths and divided by heat structures representing the VV bottom, the divertor, the VV side, and the Breeding Blanket (BB) sector. In total 5 Control Volumes (CV) have been used, each representing:

- plasma chamber (vol. 2466 m^3);
- upper port (vol. 1500 m^3);
- lower port (vol 2000 m^3);
- a volume between the divertor and the VV structure (vol. 280 m^3);
- a volume between the back of BB modules and VV structure (vol. 2000 m^3).

Fig. 2 shows the MELCOR nodalization scheme of the Vacuum Vessel volumes and heat structures.

3.3. Vacuum vessel pressure suppression system

The VVPSS consists of a series of Suppression Tanks (ST) filled with a liquid pool and an inert gas composed of nitrogen. One Bleeding Line (BL) connects the VV to the corresponding ST-A through a non-return valve that opens at a specified pressure set point. A series of lines, opened in this case by a Rupture Disk (RD), connect the VV to the other STs. The VVPSS serves as a protection to pressure peaks for the VV, keeping the maximum pressure inside the VV below 0.2 MPa. Another function of the VVPSS is to mitigate the hydrogen explosion risk that could deprive the confinement integrity of the VV. The position of the BLs and RDs connection towards the VVPSS has not been decided yet, depending on the space available in the ports. Considering the space available in the upper ring manifold and the recommendation by ITER to avoid to use the NBI ports to connect the RDs, it is here proposed to connect the RDs and BV lines to the upper ring manifold and route the relief line to the tanks placed in the lower part of the tokamak building. The tank A, referenced in the paper as Suppression Tank A (ST-A) is characterized by a minor volume (300 m^3) in wet condition, where the spurges of the bleeding lines will condensate the steam coming from the VV during LOCA conditions. The other tanks from B to F, referenced in the paper as Suppression Tank B to F, addresses the pressure peak and the steam coming from the VV in the case of the opening of the BRs. In all the tank, the preliminary water level was set up at 3.96 m condensing the major amount of the steam without a significant increase of the PSS pressure compared to the VV (around 1.9 bar) [10]. Fig. 3 shows a preliminary concept of the VVPSS layout, the proposed location in the DEMO building environments is showed in Fig. 4 and in Fig. 5.

Hydrogen mitigation represents a challenge since the VV and VVPSS have significantly different thermo-hydraulic from the application and solutions adopted for fission technologies. In the new proposed design for the VVPSS, the atmosphere composition of suppression tank has been changed by filling it with inert gas. This allow us to avoid reaching hazardous gas compositions also in the absence of PARs. However, new volumes (expansion tanks) are needed for the recombination. In the

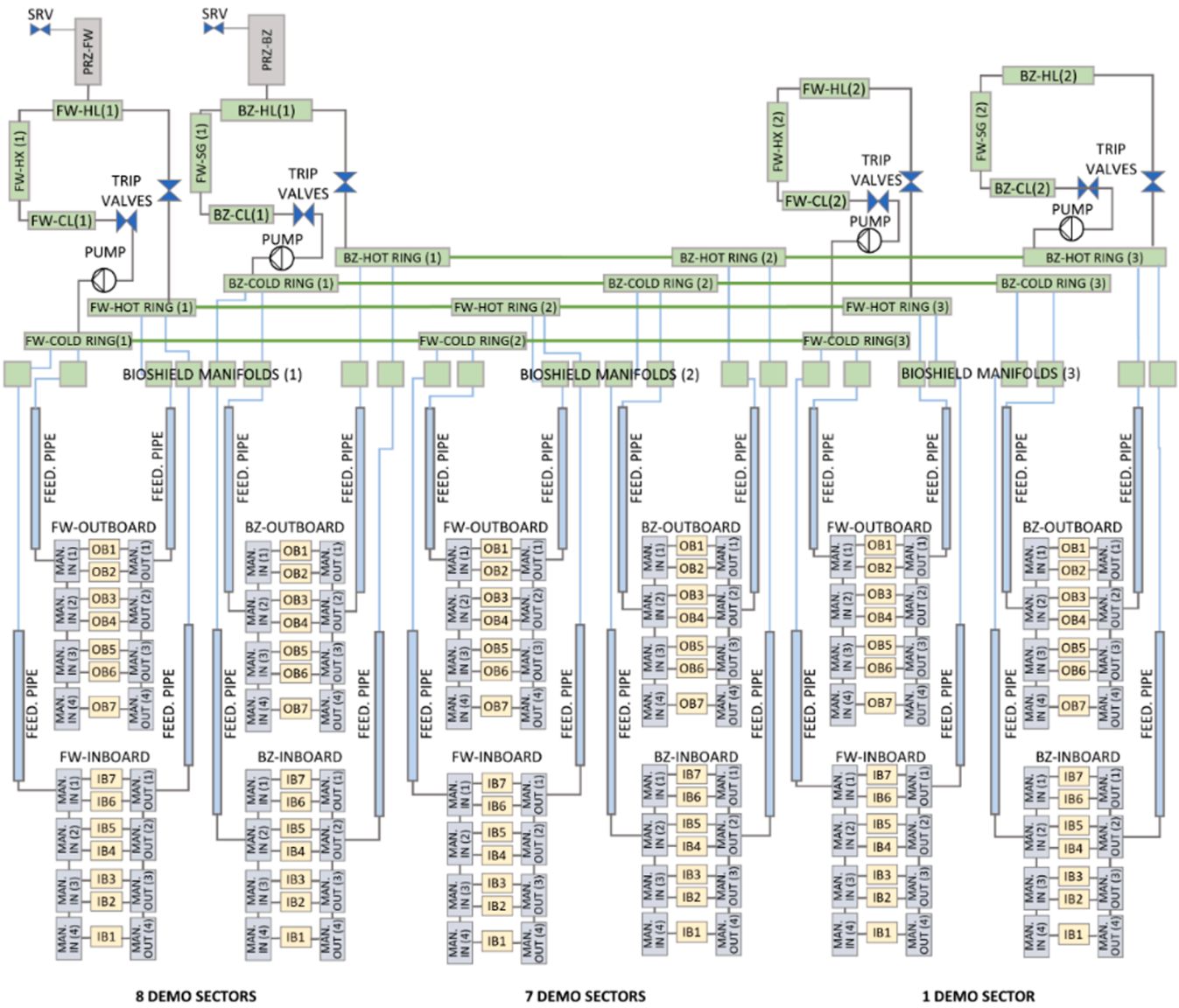

Fig. 1. Thermal hydraulic MELCOR nodalization scheme of the DEMO reactor.

proposed arrangement, two PARs are installed in Expansion Tanks (ET) one connected to the ST-A and the other connected to the ST-B. The behavior of the PAR system has been modeled through the MELCOR ESF package. The goal is to reduce the hydrogen concentration to avoid deflagration or detonation. The selected PAR chosen for this study is the AREVA FR1–150 [28], which main parameters are reported in Table 3.

The experimental campaign THAI [29,30] has obtained a correlation to evaluate the amount of hydrogen combined per unit time evaluated as:

$$\boldsymbol{m_{H2}} = \boldsymbol{N}\cdot\ \boldsymbol{\eta}\cdot(\boldsymbol{k_1}\cdot\boldsymbol{p}+\boldsymbol{k_2})\cdot\boldsymbol{v}\cdot\tanh(\boldsymbol{v}-\boldsymbol{min}(\boldsymbol{v_{H_2}})) \quad \text{(Eq.1)}$$

Where:

- N - number of recombiners (-);
- m_{H2} - recombination intensity (g/s);
- η - recombination efficiency (-);
- v - hydrogen or oxygen concentration - see below (volume%);
- p - pressure (bar);
- k_1 - recombination empirical constant (g/(s.bar));
- k_2 - recombiner empirical constant (g/s);
- $min(v_{H_2})$ (volume%) - about 0.5% (v/v) - (starting the recombiner from 2% by volume hydrogen and above 50 °C).

In particular, the variable η defines the efficiency of the recombiner and can be determined by the condition:

$$\eta = \begin{cases} 1.0 \Leftrightarrow \dfrac{v_{H_2}}{v_{O_2}} \leq 1 \\ 0.6 \Leftrightarrow \dfrac{v_{H_2}}{v_{O_2}} > 1 \end{cases}$$

The variable v is determined by the relationship:

$$v = \begin{cases} v_{H_2} \Leftrightarrow \dfrac{v_{H_2}}{v_{O_2}} < 0.5 \\ v_{O_2} \Leftrightarrow \dfrac{v_{H_2}}{v_{O_2}} \geq 0.5 \end{cases}$$

As a conservative assumption, the η has been assumed to be 0.6. The most important functional parameters for the recombiner are evaluated through MELCOR control functions. For example, the volumetric fraction of hydrogen and oxygen is evaluated in each specific suppression tank. While the m_{H2} is evaluated by MELCOR considering the pressure in the ST.

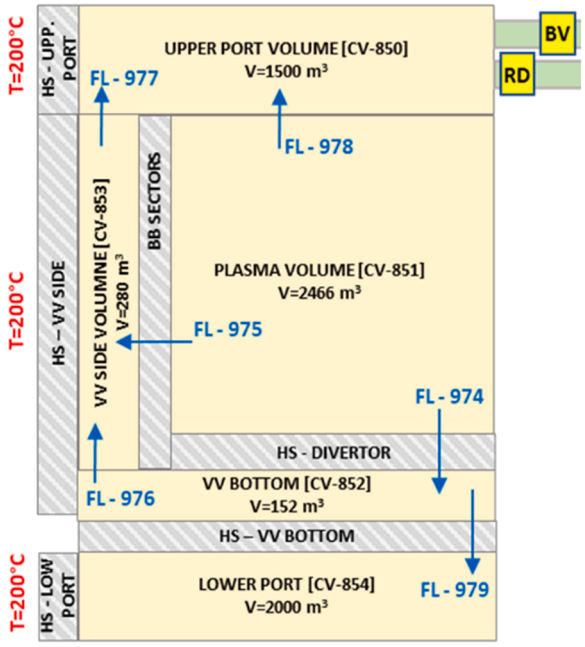

Fig. 2. MELCOR Vacuum Vessel nodalization scheme.

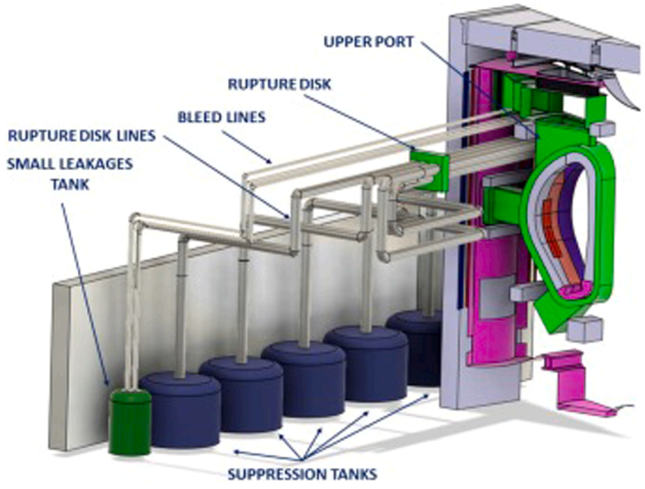

Fig. 3. Current VVPSS layout.

The hydrogen reaction rate for a single PAR unit is evaluated by the MELCOR ESF-PAR package using:

$$R_H = \eta \cdot \rho_H \cdot Q\, f(t) \qquad \text{(Eq.2)}$$

Where:

1 R_H is the hydrogen reaction rate (kg/s);
2 ρ_H is the hydrogen density of entering gas (kg/m^3);
3 η is the hydrogen reaction efficiency;
4 Q is the total gas-phase volumetric flow rate through the unit (m^3/s).

Q and η parameters should be evaluated and passed to the ESF-PAR package model to evaluate the R_H. Considering that Q is given for FR1–150 and R_H is evaluated by Eq.1, and the η parameter is evaluated from Eq. 2 using custom CFs in the MELCOR input deck. In such a way, the PARs are allowed to remove hydrogen following Eq.1.

In terms of hydrogen risk of detonation or deflagration, the VVPSS solution adopted for this analysis (shown in Fig. 6) has been verified in [31]. Results from [31] demonstrate how the proposed solution of the PAR installed in ET, significantly reduced the hydrogen explosion compared to the solution that adopts the PAR in the ST.

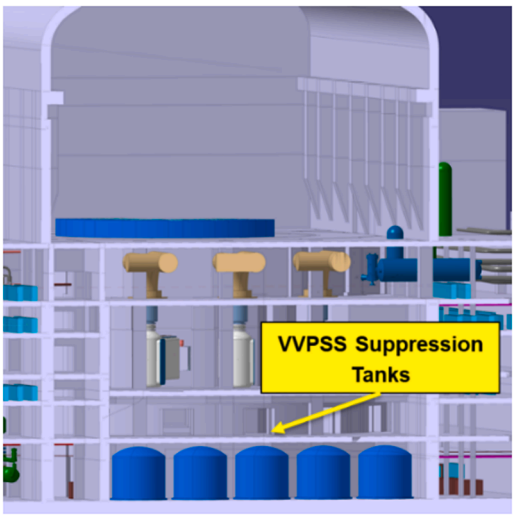

Fig. 4. VVPSS suppression tanks inside the tokamak building.

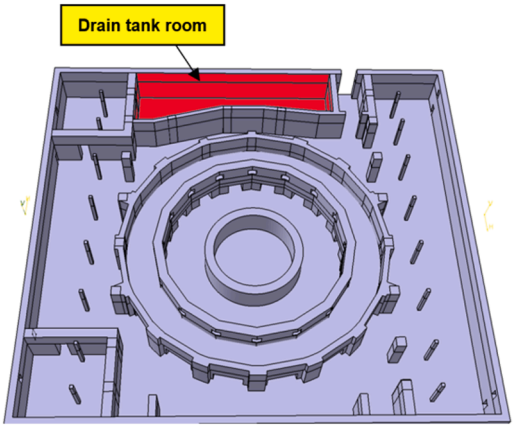

Fig. 5. Tokamak building basement level with drain tank room available volume in red.

Table 3
Recombiner Parameters [28].

Parameter	FR1–150
Length (mm)	200
Thickness (mm)	166
Height (mm)	1000
Weight (kg) approximately	18
Number of recombiner plates	15
Flow inlet at 100 kPa and 60 °C (m^3/h)	50
Recombine Volume (kg/h) for 150 kPa and 4% volume hydrogen concentration	0.18

4. RAVEN optimization strategy

The proposed VVPSS hydrogen recombination system has two PARs installed in two separated ET. The objective function chosen is the cumulative mass of hydrogen recombined by both recombiners. Considering the dependencies expressed in Eq. 1, the selected thermal-hydraulic and geometrical parameters to be optimized are:

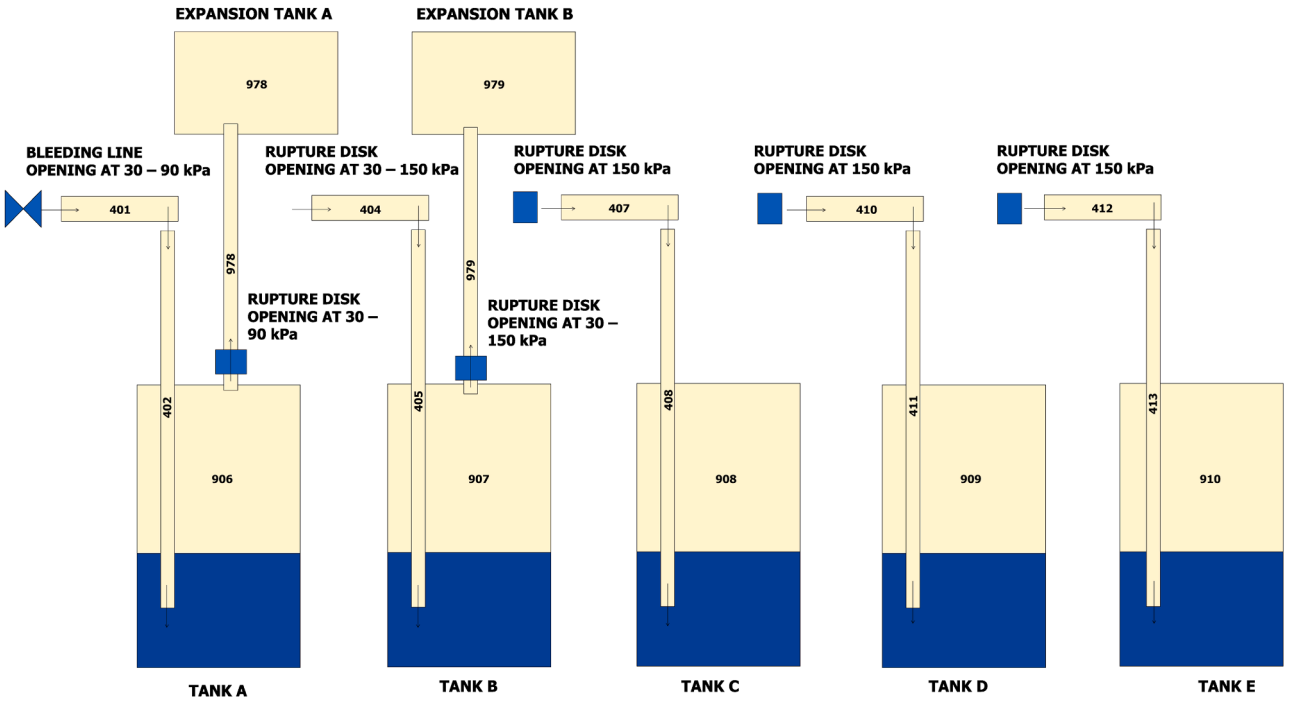

Fig. 6. VVPSS nodalization scheme.

1 Rupture Disk pressure set point (Pa);
2 Bleeding Line pressure set point (Pa);
3 Liquid Level of Suppression Tank A (m);
4 Liquid Level of Suppression Tank B (m);
5 Expansion Tanks volume (m^3).

Each parameter chosen has a limited range of variability to avoid incoherent results with the physical nature of the problem.

As reported in Section 2, the deterministic approach adopted for the optimizer may cause entrapment in local optima; therefore, several initial trajectories are selected to explore the input space globally. Table 4 shows the initial trajectory selected. The criteria adopted for the initial values are random to provide the broadest range of possible initial trajectories.

The optimization is based on the gradient descent method and the estimation technique adopted is the central difference approximation. For each trajectory a set of parameters are predicted forming one optimal candidate. MELCOR evaluates at the end of the simulation an objective function for each of the optimal candidates. The corresponding objective function is the final amount of hydrogen recombined. Consequently, RAVEN launches 2 N MELCOR simulations (*N* is the number of parameters considered in the optimization process) in parallel to the optimal candidate simulation to estimate the local gradient. At the end of each iteration the local gradient is estimated and if the acceptance criteria are not met, a new optimal candidate is determined using the gradient history iterative stepping algorithm. The acceptance criteria selected are:

- Gradient value < 1.0e-06;
- Persistence = 10;
- Maximum number of MELCOR simulations = 4000.

The persistence criterion counts the number of times convergence should be reached before a trajectory could be considered fully converged. This criterion has been selected to avoid early false convergence.

Table 4
Initial trajectories.

Trajectory ID	BL set point (Pa)	RD set point (Pa)	ET volume (m^3)	Liq. Level Tank A (m)	Liq. Level Tank B (m)
0	3.0E+04	3.5E+04	250.0	3.93	2.80
1	3.5E+04	3.0E+04	350.0	2.80	3.93
2	4.0E+04	4.5E+04	300.0	2.30	3.30
3	4.5E+04	4.0E+04	400.0	3.30	2.30
4	5.0E+04	5.5E+04	350.0	2.80	1.80
5	5.5E+04	5.0E+04	250.0	1.80	2.80
6	3.5E+04	5.5E+04	450.0	2.30	3.30
7	5.5E+04	3.5E+04	300.0	3.30	2.30
8	4.0E+04	5.5E+04	450.0	1.80	3.93
9	5.5E+04	4.0E+04	400.0	3.93	1.80

5. Main outcomes

An in-vessel LOCA is simulated to evaluate the effectiveness of the VVPSS in terms of hydrogen recombination. The initiating event is a DEGB of 10 OB-FW cooling channels, for a total break area of 0.00098 m^2, during a plasma burn phase with resulting in-vessel LOCA. The unmitigated disruption is assumed to affect two different outboard segments causing the additional break of 262 FW channels, for a total break area of 0.02568 m^2. According to [32,33] the tritium source term is located in the dust present or deposited in the VV but also in plasma facing components. It has been assumed that the 2.673 kg of mobilizable tritium, forming part of the source term, can chemically react with the catalytic layer of the PARs [13]. As a conservative assumption, the recombination of mobilizable tritium forming tritiated water compounds has been neglected.

The Postulated Initiating Event (PIE) occurs at time 0.0 s. The water and steam mass released from the failure of FW channels is shown in Fig. 7 and Fig. 8. The trend is the same for all the simulations since the parameters to be optimized do not affect the mass flow transient entering the VV. At the end of the transient, about 66.7 tons of water and 45.46 tons of steam are discharged from FW-PHTS into the VV. The release of this amount of water and steam within the VV leads to rapid pressurization of the VV volumes causing the triggering of bleed lines and rupture discs with the mobilization of hydrogen and steam towards

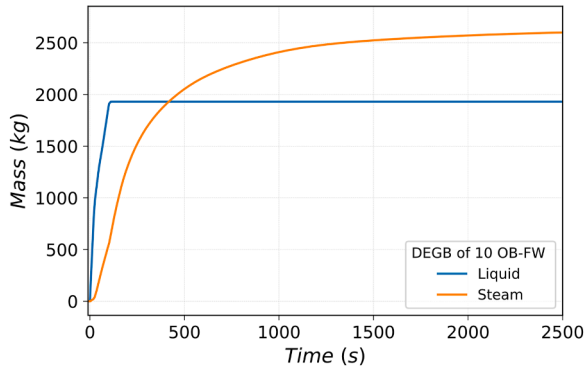

Fig. 7. Mass of water released from the DEGB of 10 OB-FW to the VV.

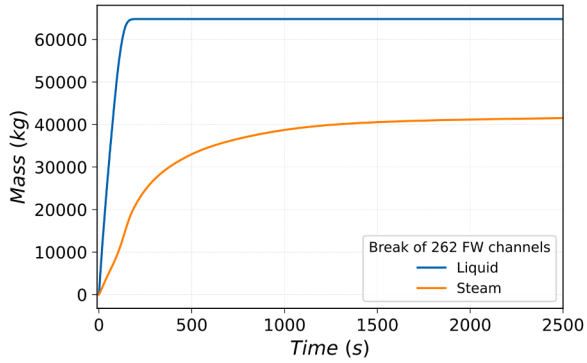

Fig. 8. Mass of water released from the break of 262 FW to the VV.

the VVPSS tanks.

The RAVEN optimizer explores 10 initial trajectories, as reported in Table 4, using the gradient descent method and a central difference gradient approximation. One iteration for each trajectory involves 11 independent MELCOR simulations, the first involves the optimal candidate, and the other 10 are needed for the central difference local gradient calculation. The total simulation time imposed is 25,000.0 s to reach a final equilibrium state in the suppression and expansion tanks and correctly evaluate the recombination process. Before reaching a satisfactory convergence, each trajectory performs several iterations, forming a total of 4000 runs. Each following figure will represent only the variables of the optimal candidates run. During the optimization process if an iteration does not reach an increase of the objective function, then it will be discarded and not represented. The trajectory with the highest number of iterations accepted is trajectory #3, totaling 17 iterations.

The final mass of recombined hydrogen explored by the optimization algorithm is shown in Fig. 9, with the corresponding final values in Table 5. For a better perspective, Fig. 9 shows only the runs of each trajectory that reach a successful optimization. All the trajectories reach a final amount of H_2 recombined restricted in a short interval. The lowest amount of hydrogen recombined by trajectory number 5 is 7.2% lower than the highest amount of hydrogen recombined by trajectory 9. The significant difference in the objective function value between the first iteration and the last converged iteration proves the effectiveness of the optimization algorithm adopted.

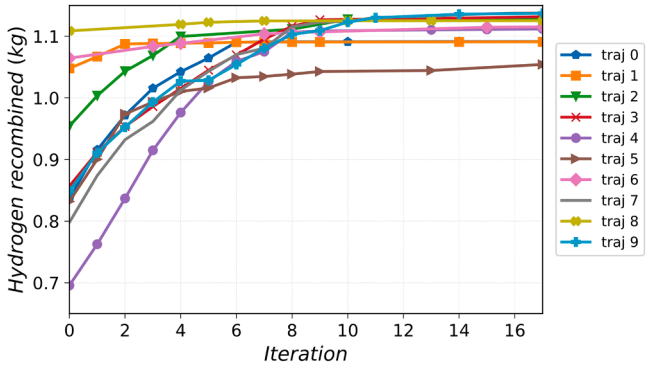

Fig. 9. Final H_2 recombined during each successful iteration.

After the in vessel LOCA occurrence, pressure in the VV increases very quickly. From this point, the optimization study on the BL and the RD setpoint outlines different sequences. As soon as the fixed pressure setpoints are reached, steam and hydrogen are discharged in ST-A and ST-B. The VV pressure is ulteriorly mitigated by opening the remaining RDs (opening a path towards the ST-C to ST-E) at a fixed set point of 150 kPa. The pressure suppression system limits the maximum pressure to 150 kPa (below the design pressure of 200 kPa). After opening all RDs, the pressure inside the VV starts to decrease since the steam from the FW-PHTS is condensed inside the suppression tanks.

The first optimization parameters shown are the BL and RD set points, in Fig. 10 and Fig. 11, divided into trajectories for each step taken by the optimization algorithm. The main difference between the BL and RD lines concerns their flow area. The RD line has an opening of 1.6 m^2, while the BL line has a smaller opening equal to 0.6 m^2. The RD and BL setpoints affect the amount of hydrogen discharged in the STs, and, consequently, the available amount of hydrogen that could be recombined in the ETs.

Fig. 12 shows the amount of H_2 discharged in the ET-A, while Fig. 13 shows the amount of H_2 discharged in Tank-B. Four different approaches could be discretized for the BL and RD set point final converged values:

1 BL set point $\sim$ 90 kPa and RD set point $\sim$ 30 kPa;
2 BL set point $<$ 40 kPa and RD set point $<$ 40 kPa;
3 BL set point $<$ 40 kPa and RD set point $>$ 40 kPa;
4 BL set point $>$ 50 kPa and RD set point $>$ 50 kPa.

The first discretize group of trajectories settles the lowest value for the RD and the highest values for the BL to take advantage of the higher discharge capability of the RD line. Consequently, the hydrogen discharged in the ET-B is significantly increased, as shown in Fig. 13. This strategy has a negative counterpart regarding the PAR in the ET-A, which is never triggered. The condition set on the minimum hydrogen concentration in the atmosphere is not respected; therefore, the recombiner is inactive. Nevertheless, a considerable amount of hydrogen is discharged towards the ET-A, on average 0.1 kg. This could represent a risk of deflagration or detonation involving hydrogen buildup in an atmosphere with the presence of oxygen. This approach should be applied differently by involving just one PAR installed in the ET-B and removing the ET-A.

The second and third sets of trajectories follow a similar approach to the set described above regarding the RD set point, although they differ on the BL set point. The approach is to take advantage of the high

Table 5
Final optimized H_2 recombined.

trajectory	Final amount of H_2 estimated by the optimization algorithm (kg)
0	1.091
1	1.090
2	1.128
3	1.132
4	1.111
5	1.054
6	1.115
7	1.137
8	1.125
9	1.137

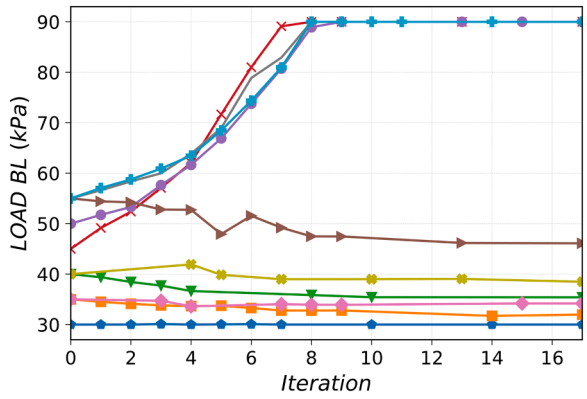

Fig. 10. BL set point during the optimization process.

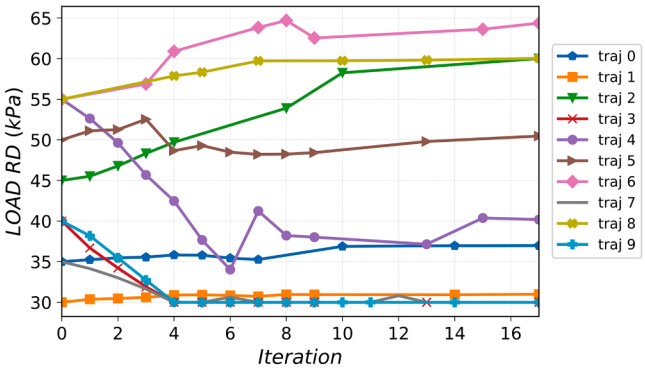

Fig. 11. RD set point during the optimization process.

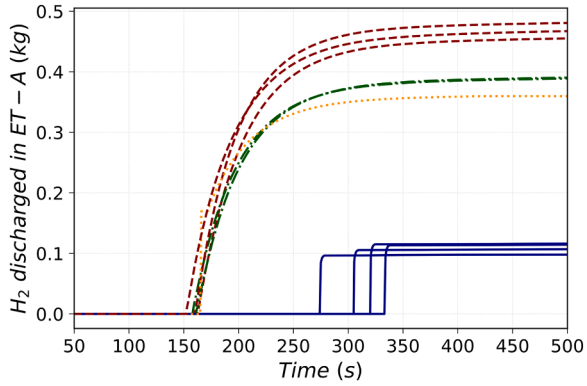

Fig. 12. Hydrogen discharged towards ET-A.

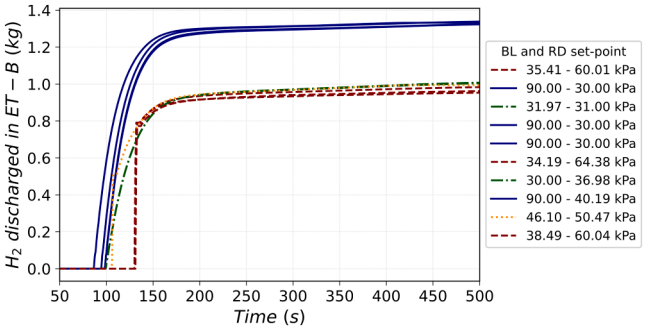

Fig. 13. Hydrogen discharged towards ET-B.

discharge capability of the RD line but also benefit from the presence of the ET-A. Consequently, the set point of the BL is decreased in the range of the RD set point. As a result, the hydrogen concentration inside the ET-A reaches the minimum concentration limit, and the PAR is activated. Compared with the first set, the second and third set decreases the amount of hydrogen recombined by the PAR in the ET-B but has the other PAR active in ET-A.

The last set of trajectories ulteriorly favors the discharge towards ST-A by setting a lower set point value for the BL than the set point of RD line. Even though the BL opens before, the greater flow path area of the RD line determines a higher amount of hydrogen discharged in ET-B. Compared to the set before, it increases on average by 25% the amount of hydrogen discharged in ET-A while maintaining the same amount of hydrogen discharged towards the ET-B.

Fig. 14 depicts the amount of hydrogen discharged in both ET. Although the optimization approaches are different and even opposite, the final amount of hydrogen discharged in the ET is almost equal. Another important aspect to analyze is the possible buildup of H_2 inside the ETs. An efficient system would discharge the highest amount of hydrogen from the ST to the ET and recombine the highest amount of hydrogen discharged. Fig. 15 shows the ratio between the hydrogen recombined in the ETs and the H_2 final amount recombined in the ETs. All the four different approaches reach an efficient discharge ratio.

Table 6 summarizes the final amount of hydrogen discharged in the ETs and the ratio between the amount of hydrogen discharged in the ET and the hydrogen recombined for each trajectory.

The liquid level optimization steps inside the Tank-A do not show any trend or convergence towards a specific value. Instead, the optimization search for the liquid level inside the ST-B shows convergence towards the highest liquid level possible inside the tank. Fig. 16 shows the Liquid Level in ST-A for each trajectory, and Fig. 17 shows the liquid level in ST-B for each trajectory explored by the optimization algorithm.

The liquid level parameter affects the pressure transient inside the tank, and the hydrogen concentration, both directly correlated to the hydrogen recombined rate as shown in Eq. 1. The suppression of steam inside the ST is directly influenced by the liquid level. A higher liquid level coincides with a more effective pressure suppression. A lower liquid level coincides with a less effective suppression and, therefore, a higher-pressure transient inside the suppression tank. The liquid level similarly affects the hydrogen concentration inside ET-B. Since hydrogen is a non-condensable gas, more effective suppression of steam corresponds to a higher amount of hydrogen per unit volume released towards the ET-B.

The pressure transient and the hydrogen concentration are both affected by the liquid level but are in opposition to one another. A lower liquid level inside the ST corresponds to a higher-pressure transient in the ST and a lower amount of hydrogen per unit volume released towards the ET. At the same, as shown in Eq. 1, the pressure and the hydrogen concentration are directly proportional to the rate of hydrogen

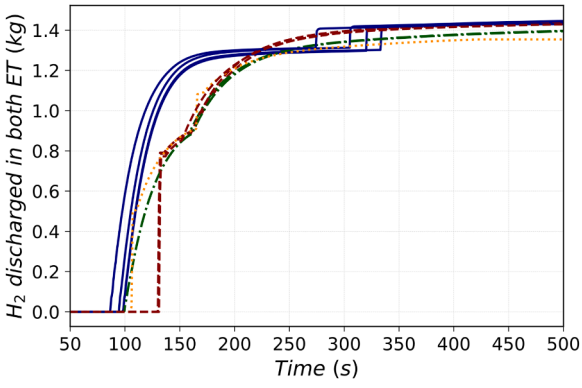

Fig. 14. Hydrogen discharged towards both ET.

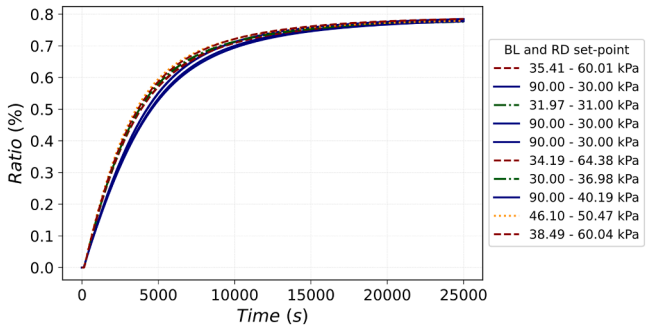

Fig. 15. Ratio between the amount of H_2 discharged in the ET and the H_2 recombined.

Table 6
Hydrogen discharged in both ET and Ratio with corresponding setpoint values.

trajectory	Final amount of H_2 discharged in the ETs (kg)	Ratio of H_2 discharged and recombined in the ETs (%)	BL set point (Pa)	RD set point (Pa)
0	1.405	0.776	3.01E+04	3.69E+04
1	1.405	0.776	3.20E+04	3.09E+04
2	1.446	0.779	3.54E+04	6.0E+04
3	1.450	0.780	9.00E+04	3.0E+04
4	1.430	0.777	9.00E+04	4.02E+04
5	1.353	0.778	4.61E+04	5.05E+04
6	1.435	0.777	3.42E+04	6.44E+04
7	1.450	0.784	9.00E+04	3.0E+04
8	1.433	0.785	3.85E+04	6.0E+04
9	1.450	0.785	9.00E+04	3.0E+04

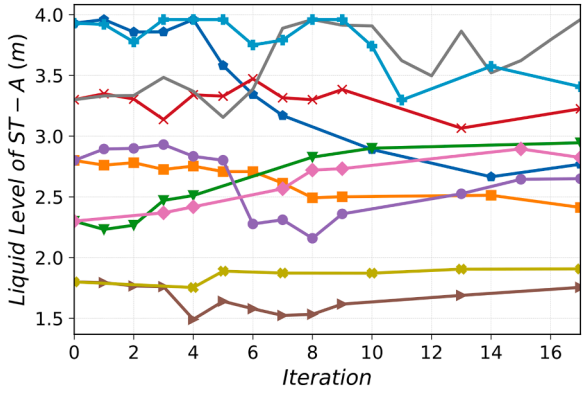

Fig. 16. Liquid level of ST-A during the optimization process.

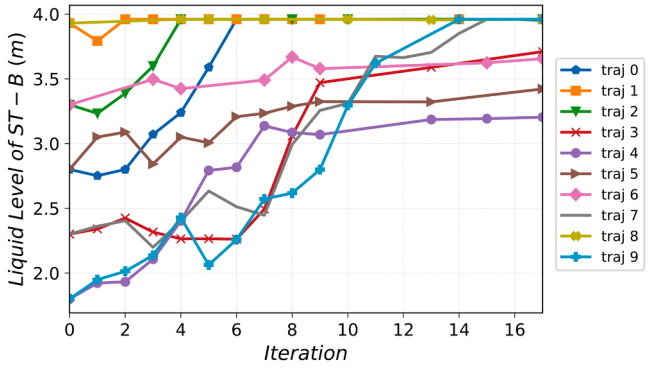

Fig. 17. Liquid level of ST-B during the optimization process.

recombined by the PAR system. Between the two, the hydrogen concentration inside the ET-B has a higher influence than the pressure inside the recombiner volume. Therefore, the optimization algorithm tends to increase the hydrogen volume concentration instead of the pressure, increasing the liquid level inside the ST-B.

The following Figs. 18-21 show the hydrogen concentration transient of the ET-B of several trajectories. For graphical reasons, only four trajectories are displayed with their respective iteration. The final optimized iteration for each trajectory is highlighted, while the previous, not optimized iterations are faded. As the optimization algorithm increases the liquid level for all the trajectories, the hydrogen concentration increases accordingly, underlying the correlation between both variables.

Fig. 22 shows the expansion tanks free volume for each trajectory explored by the optimization algorithm. The optimization algorithm found two values:

1 ET volume ~ 450 m^3;
2 ET volume ~ 580 m^3.

The ET volume parameter is directly involved with the hydrogen volume concentration. Fig. 23 shows two distinctive trends for the hydrogen volume concentration associated with the two strategies adopted by the optimization algorithm.

The trajectories that resulted in an ET volume equal to 570 – 580 m^3 correspond to those strategies where the PAR installed in ET-A is inactive. In comparison, the other trend that sets the ET volume equal to 450 m^3 corresponds to strategies with both PARs active. Figs. 24 and 25 present the hydrogen recombined in both the ET, respectively, underlying the connection between the strategy where the PAR is active or not and its optimized ET volume.

The final converged values associated with the parameters investigated and the corresponding amount of hydrogen recombined are summarized in Table 7. In terms of the amount of hydrogen recombined, the most efficient approaches take advantage of the different flow areas of the RD line rather than the BL. Therefore, only the ET-B is active with a corresponding volume equal to 580 m^3, and the liquid level of ST-B is at 3.96 m. This strategy, if adopted, should remove the presence of the ET-A to exclude risks of deflagration or detonation in its oxygenated atmosphere where hydrogen is discharged.

6. Summary and conclusions

The RAVEN optimizer algorithm, based on the gradient descent method, has been employed on the thermal-hydraulic parameters of the PAR system installed in the VVPSS of DEMO to maximize the amount of hydrogen recombined. The initiating event imposed to test the VVPSS capabilities is a DEGB of 10 OB-FW cooling channels resulting in an in-vessel LOCA modeled in MELCOR. The unmitigated disruption is assumed to affect two different outboard segments causing the additional break of 262 FW channels. The optimization pursual revealed that

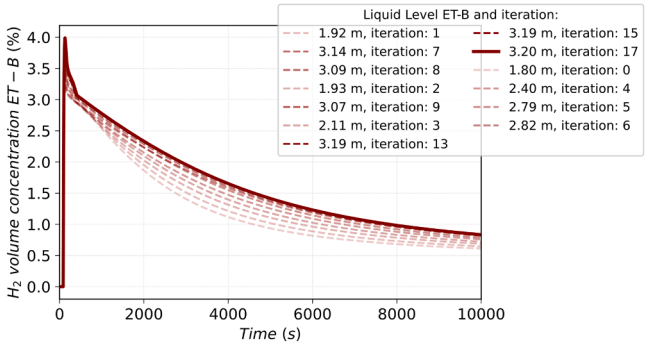

Fig. 18. Hydrogen volume concentration of ET-B for trajectory 4.

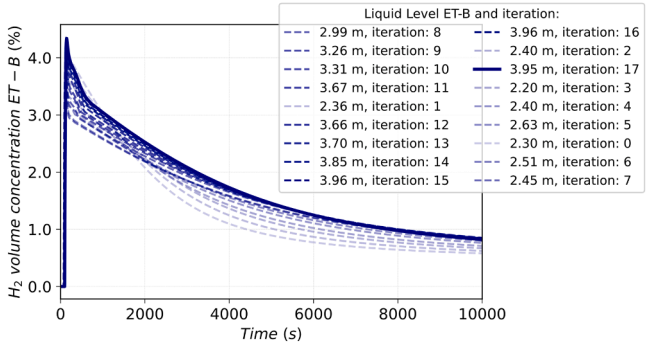

Fig. 19. Hydrogen volume concentration of ET-B for trajectory 7.

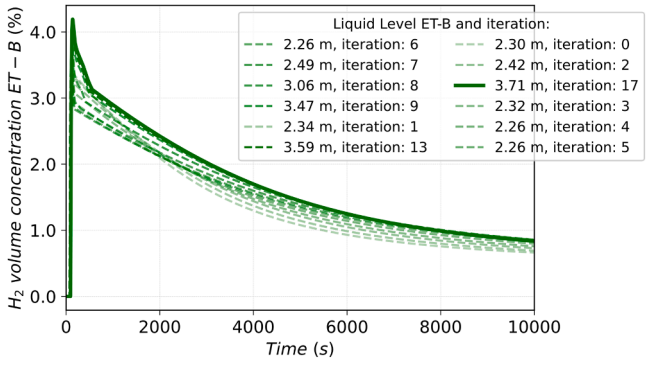

Fig. 20. Hydrogen volume concentration of ET-B for trajectory 3.

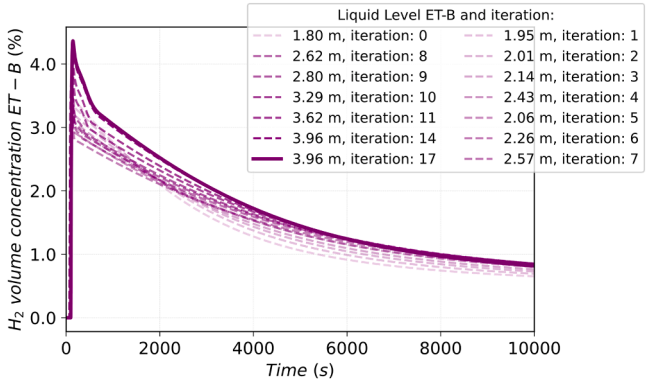

Fig. 21. Hydrogen volume concentration of ET-B for trajectory 5.

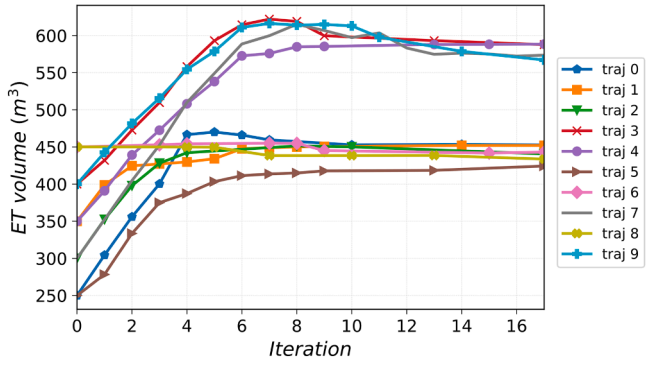

Fig. 22. Expansion Tank volume during the optimization process.

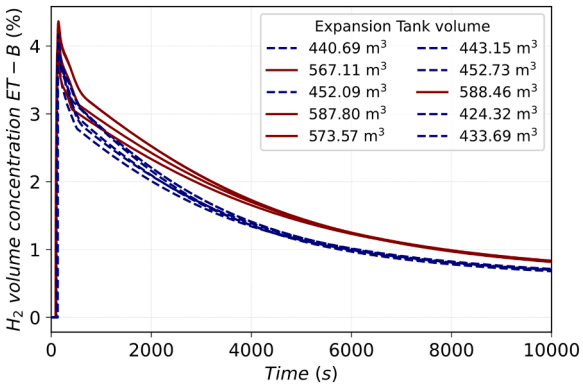

Fig. 23. Hydrogen volume concentration inside ET-B discretized between ET strategies.

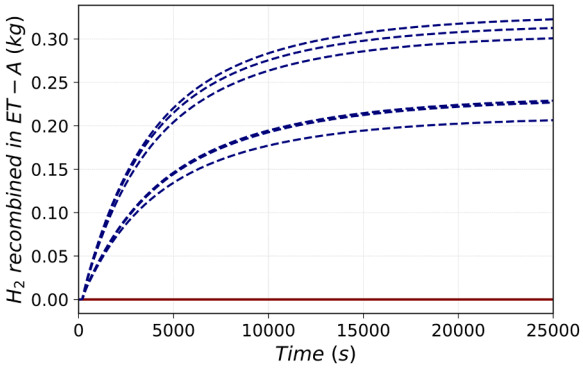

Fig. 24. Hydrogen recombined in ET-A divided between trajectory final optimal candidates.

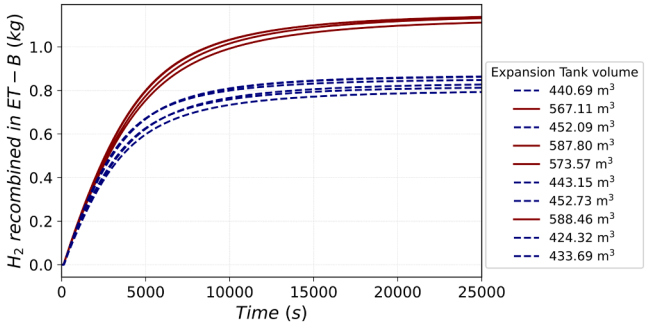

Fig. 25. Hydrogen recombined in ET-B divided between trajectory final optimal candidates.

different strategies could be adopted, having each a similar maximized amount of hydrogen recombined. The system parameters investigated are the BL and RD pressure set point for opening the liquid level inside the ST-A and ST-B, and the volume of the expansion tanks where the PARs are installed. Ten initial trajectories are carried out independently to avoid the entrapment in a local maximum with a low level of hydrogen recombined. The highest amount of iteration needed before reaching a satisfactory convergence is 17 successful iterations; in total, 4000 MELCOR runs are performed. The central different approximation adopted has a precise evaluation of the local gradient, although it lacks calculation time efficiency because it needs 2n parallel simulation to evaluate the local gradient (where n is the number of parameters involved in the optimization).

The results showed an interesting approach that could be adopted by

Table 7
Initial and final converged values for each trajectory.

Trajectory ID		BL set point (Pa)	RD set point (Pa)	ET volume (m^3)	Liq. Level Tank A (m)	Liq. Level Tank B (m)	H_2 recombined (kg)
0	Initial	3.0E+04	3.5E+04	250.0	3.93	2.80	0.836
	Converged	3.01E+04	3.69E+04	452.72	2.77	3.96	1.091
1	Initial	3.5E+04	3.0E+04	350.0	2.80	3.93	1.047
	Converged	3.2E+04	3.09E+04	452.09	2.41	3.96	1.091
2	Initial	4.0E+04	4.5E+04	300.0	2.30	3.30	0.954
	Converged	3.54E+04	6.0E+04	440.68	2.95	3.96	1.127
3	Initial	4.5E+04	4.0E+04	400.0	3.30	2.30	0.856
	Converged	9.0E+04	3.0E+04	587.80	3.23	3.71	1.131
4	Initial	5.0E+04	5.5E+04	350.0	2.80	1.80	0.695
	Converged	9.0E+04	4.02E+04	588.46	2.65	3.30	1.111
5	Initial	5.5E+04	5.0E+04	250.0	1.80	2.80	0.831
	Converged	4.61E+04	5.05E+04	424.31	1.76	3.43	1.054
6	Initial	3.5E+04	5.5E+04	450.0	2.30	3.30	1.064
	Converged	3.42E+04	6.44E+04	443.15	2.83	3.70	1.115
7	Initial	5.5E+04	3.5E+04	300.0	3.30	2.30	0.797
	Converged	9.0E+04	3.0E+04	573.57	3.96	3.95	1.137
8	Initial	4.0E+04	5.5E+4	450.0	1.80	3.93	1.108
	Converged	3.85E+04	6.0E+04	433.69	1.91	3.96	1.125
9	Initial	5.5E+04	4.0E+04	400.0	3.93	1.80	0.840
	Converged	9.0E+04	3.0E+04	567.11	3.41	3.96	1.137

increasing the BL set point to 90 kPa and setting the lowest set point for the RD at 30 kPa. The recombiner installed could be reduced to just one, the ET-B, because in this scenario, most of the hydrogen is discharged in the ST-B and small quantities in the ST-A. The consequential low hydrogen volume concentration value in the ET-A does not reach the threshold to activate the PAR, making its installment worthless. A different approach with similar hydrogen recombination results is to set the lowest set point for the BL and the RD set point at 60 kPa. This strategy permits an efficient usage of both recombiners. The preliminary design of the VVPSS mitigates the pressure transient opening first the BL and if needed the intervention of the RD suppress definitely the pressure peak of the VV in case of in-vessel LOCA. The optimization presented in this paper however highlights to designers a different procedure that could be adopted for the BL and RD operational logic in terms of hydrogen recombination through passive recombiner in contrast with a first design concept. New studies could be performed focusing on a different strategy of the VVPSS to mitigate pressure transient in the VV, including the results presented in the paper and the level reached at the design level.

The final converged value of the liquid level inside the suppression tank B reached a similar value for all the different trajectories, establishing the strategy to follow. The value is set at the highest liquid level available for the ST-B to suppress the highest amount of steam, therefore increasing the hydrogen volume concentration in the tank's atmosphere. The optimization study involving the liquid level on ST-A has not shown any evident convergence trend.

The expansion tank volume has been optimized towards two different values, 450 m^3 and 580 m^3. The lower volume is associated with the approach where both recombiners are active, while the higher volume has been optimized for the approach where only one PAR is active.

Of the assumed 2.673 kg of mobilizable tritium forming part of the source term that can chemically react with the catalytic layer of the PARs, the highest amount of hydrogen recombined is 1.137 kg. The associated trajectory is the number 9, characterized by the lowest set point for the RD at 30 kPa and the highest available set point for the BL at 90 kPa. Thus, the PAR installed in ET-A is inactive for this trajectory. The liquid level of ST-B is set at the highest possible, and the expansion tank volume has been set at 560 m^3.

This work demonstrated the capabilities of RAVEN in optimizing a general objective function. The gradient descent method allows precise estimation of optima, although it entraps easily in local maximum or minimum when evaluating a multimodal objective function. Initializing the search with parallel trajectories helps with avoiding local entrapment, although it does not solve the natural flaw of the algorithm when applied to multimodal problems. Future developments could involve the integration between a stochastic search of the input space and the gradient descent method applied to the most prominent runs. This hybrid algorithm would take advantage only of the best features of both methods overcoming their intrinsic flaws.

Abbreviations

BB	Breeding Blanket
BL	Bleeding Line
BZ	Breeding Zone
CV	Control Volume
DBA	Design Basis Accident
DEGB	Double Ended Guillotine Break
FW	First Wall
ET	Expansion Tank
INL	Idaho National Laboratory
LOCA	Loss of Coolant Accident
OB-FW	Outboard First Wall
PAR	Passive Autocatalytic Recombiners
PHTS	Primary Heat Transfer System
PIE	Postulated Initiating Event
RD	Rupture Disk
SPSA	Simultaneous Perturbation Stochastic Approximation
ST	Suppression Tanks
VV	Vacuum Vessel
VVPSS	Vacuum Vessel Pressure Suppression System
WCLL	Water-Cooled Lithium Lead
WPSAE	Work Package Safety And Environement

Declaration of Competing Interest

The authors declare that they have no known competing financial interests or personal relationships that could have appeared to influence the work reported in this paper.

Data availability

The data that has been used is confidential.

Acknowledgments

This work has been carried out within the framework of the EUROfusion Consortium, funded by the European Union via the Euratom

Research and Training Program (Grant Agreement No 101052200 — EUROfusion). Views and opinions expressed are however those of the author(s) only and do not necessarily reflect those of the European Union or the European Commission. Neither the European Union nor the European Commission can be held responsible for them. The work of M. D'Onorio has been financially supported by a EUROfusion Engineering Grant.

References

[1] N. Taylor, et al., Safety and environment studies for a European DEMO design concept, Fusion Eng. Des. 146 (2019), https://doi.org/10.1016/j.fusengdes.2018.11.049.
[2] G. Caruso, et al., DEMO – the main achievements of the Pre – concept phase of the safety and environmental work package and the development of the GSSR, Fusion Eng. Des. (2022), https://doi.org/10.1016/j.fusengdes.2022.113025.
[3] T. Pinna, et al., Identification of accident sequences for the DEMO plant, Fusion Eng. Des. (2017), https://doi.org/10.1016/j.fusengdes.2017.02.026.
[4] M.T. Porfiri, et al., Safety assessment for EU DEMO – achievements and open issues in view of a generic site safety report, Fusion Eng. Des. 155 (2020), https://doi.org/10.1016/j.fusengdes.2020.111541. Article 111541.
[5] M. D'Onorio, et al., Preliminary safety analysis of an in-vessel LOCA for the EU-DEMO WCLL blanket concept, Fusion Eng. Des. 155 (2020), https://doi.org/10.1016/j.fusengdes.2020.111560. Article 111560.
[6] A. Del Nevo, et al., Recent progress in developing a feasible and integrated conceptual design of the WCLL BB in EUROfusion project, Fusion Eng. Des. 146 (2019), https://doi.org/10.1016/j.fusengdes.2019.03.040.
[7] I. Moscato, et al., Tokamak cooling systems and power conversion system options, Fusion Eng. Des. 178 (2022), https://doi.org/10.1016/j.fusengdes.2022.113093.
[8] S. Ciattaglia, et al., EU DEMO safety and balance of plant design and operating requirements. Issues and possible solutions, Fusion Eng. Des. 146 (2019) 2184–2188, https://doi.org/10.1016/j.fusengdes.2019.03.149.
[9] T. Pinna, et al., Safety important classification of EU DEMO components, Fusion Eng. Des. 146 (2019), https://doi.org/10.1016/j.fusengdes.2019.01.040.
[10] M. D'Onorio, G. Caruso, Pressure suppression system influence on vacuum vessel thermal-hydraulics and on source term mobilization during a multiple first Wall – Blanket pipe break, Fusion Eng. Des. 164 (2021), https://doi.org/10.1016/j.fusengdes.2020.112224.
[11] G. Caruso, et al., Sizing of the vacuum vessel pressure suppression system of a fusion reactor based on a water-cooled blanket, for the purpose of the preconceptual design, Sci. Technol. Nucl. Install. (2016), https://doi.org/10.1155/2016/8719695. Article 8719695.
[12] G. Mazzini et al., Hydrogen explosion mitigation in DEMO vacuum vessel pressure suppression system using passive recombiners, (2021), https://doi.org/10.1016/j.fusengdes.2021.112713.
[13] G. Mazzini, et al., Estimation of tritium and dust source term in european DEMOnstration fusion reactor during accident scenarios, J. Nucl. Rad. Sci. (2019), https://doi.org/10.1115/1.4043379.
[14] C. Rabiti, et al., RAVEN User Manual, Battelle Energy, Alliance, Idaho Falls, IS, USA, 2019.
[15] A. Alfonsi, D. Mandelli, Mutual integration of classical and dynamic PRA, Nucl. Technol. 207 (3) (2020) 363–375, https://doi.org/10.1080/00295450.2020.1776030.
[16] M. D'Onorio, et al., Dynamic event tree analysis as a tool for risk assessment in nuclear fusion plants using RAVEN and MELCOR, IEEE Trans. Plasma Sci. (2022), https://doi.org/10.1109/TPS.2022.3165170.
[17] M. D'Onorio, et al., Preliminary uncertainty quantification of the core degradation models in predicting the Fukushima Daiichi unit 3 severe accident, Nucl. Eng. Des. (2021), https://doi.org/10.1016/j.nucengdes.2021.111383.
[18] M. D'Onorio, et al., Severe accident sensitivity and uncertainty estimation using MELCOR and RAVEN, J. Phys. Conf. Ser. (2022), https://doi.org/10.1088/1742-6596/2177/1/012021.
[19] R.O. Gauntt, et al., MELCOR computer code manuals vol. 1: primer and users guide version 1.8.6, NUREG/CR-6119, vol. 1, Rev. 3, Sandia Nal. Lab. (2005).
[20] J. Merrill, et al., A recent version of MELCOR for fusion safety applications, Fusion Eng. Des. 85 (2010) 1479–1483, https://doi.org/10.1016/j.fusengdes.2010.04.017.
[21] A. Faramarzi, et al., Equilibrium optimizer: a novel optimization algorithm, Knowl. Based Syst. (2020), https://doi.org/10.1016/j.knosys.2019.105190.
[22] D.G. Luenberger, Linear and Nonlinear Programming, 2nd ed., Addison-Wesley, 1984. https://web.stanford.edu/class/msande310/310trialtext.pdf.
[23] S. Boyd, L. Vandenberghe, Convex Optimization, Cambridge University Press, Cambridge, U.K, 2004. https://web.stanford.edu/~boyd/cvxbook/bv_cvxbook.pdf.
[24] A. Faramarzi, M.H. Afshar, A novel hybrid cellular automata–linear programming approach for the optimal sizing of planar truss structures, Civ. Eng. Environ. Syst. 31 (2014) 209–228, https://doi.org/10.1080/10286608.2013.820280.
[25] A. Faramarzi, M.H. Afshar, Application of cellular automata to size and topology optimization of truss structures, Sci. Iran. 19 (2012) 373–380, https://doi.org/10.1016/j.scient.2012.04.009.
[26] S. Mirjalili, et al., Grey wolf optimizer, Adv. Eng. Softw. 69 (2014) 46–61, https://doi.org/10.1016/j.advengsoft.2013.12.007.
[27] G.A. Spagnuolo Integrated design of breeding blanket and ancillary systems related to the use of helium or water as a coolant and impact on the overall plant design, Fusion Eng. Des., https://doi.org/10.1016/j.fusengdes.2021.112933.
[28] M. Kotouč, Výstupy a doporučení plynoucí z projektu OECD/NEA THAI-2. In Technical Report ÚJV Z-4882-T, ÚJV Řež, (2017).
[29] S. Gupta, et al., THAI test facility for experimental research on hydrogen and fission product behaviour in light water reactor containments, Nuclear Eng. Des. 2015 294 (2015), https://doi.org/10.1016/j.nucengdes.2015.09.013.
[30] A. Flores, et al., Analyses of THAI 1 hydrogen deflagration using MELCOR code version 2.1 and 2.2, Nuclear Eng. Des. 369 (2020), 110838, https://doi.org/10.1016/j.nucengdes.2020.110838.
[31] M. D'Onorio et al., Passive hydrogen recombination during a beyond design ba-ses accident in a fusion DEMO plant, energies - water coolant lithium lead breeding blanket and test blanket module: design and R&D activities in 2022, (2023), https://doi.org/10.3390/en16062569.
[32] G. Mazzini, et al., Tritium and dust source term inventory evaluation issues in the European DEMO reactor concepts, Fusion Eng. Des. (2019), https://doi.org/10.1016/j.fusengdes.2019.01.008.
[33] G. Mazzini, T. Kaliatka, M.T. Porfiri, Estimation of tritium and dust source term in european DEMOnstration fusion reactor during accident scenarios, J. Nuclear Rad. Sci. (2019), https://doi.org/10.1115/1.4043379.